

## **Chapter 3 Isothermal Lamellar Thickening in Linear Polyethylene: Correlation between the Evolution of the Degree of Crystallinity and the Melting Temperature.**

### **3.1 Introduction**

Lamellar crystals of a number of flexible polymers such as polyethylene and poly(ethylene oxide) exhibit a phenomenon known as isothermal thickening. It is believed that the segmental motions associated with their crystal  $\alpha$ -relaxation<sup>1,2</sup> enable the thickening of lamellae at high crystallization or annealing temperatures. Lamellar thickening is a spontaneous process driven by the system's attempt to reduce the overall magnitude of its crystal-liquid interfacial free energy. As lamellae thicken, they become more stable (i.e., their melting temperature increase) and the material's degree of crystallinity increases.

In this paper, we show for the first time a correlation between the increase in the degree of crystallinity (assumed to arise by lamellar thickening) and the increase in the thermal stability of these lamellae. A second outcome of this work is to show that, given a simple kinetic model of the thickening process, it is possible to deconvolute the effects of primary and secondary crystallization during isothermal crystallization. Limitations of the model are outlined.

### **3.2 Experimental Section**

A narrow molar mass linear polyethylene sample with  $M_w = 119000$  g/mol and  $M_w/M_n = 1.19$  (SRM-1184a from NIST) was used in this study as received.

The calorimetric experiments were performed in a Pyris 1 model Perkin-Elmer differential scanning calorimeter operated under dry nitrogen with an ice-water bath heat sink. For a proper accounting of thermal lag effects, temperature calibration during heating was carried out using pure metal standards (indium and tin) sandwiched between two polymer films. Heats of fusion were calibrated using the latent heat of an indium standard.

Studies of the melting behavior were carried out after isothermal crystallization using a heating rate of 10 K/min. Thin polymer films were prepared by successive compression molding at 165 °C under a pressure of 10<sup>6</sup> Pa in a Carver laboratory press under a dry nitrogen atmosphere for 5 min and quenching into an ice-water mixture. To minimize the effect of temperature gradients on the melting behavior, sample mass and thickness were kept relatively low (ca. 2.0 mg and 50 μm, respectively). The use of thin samples and the proper accounting of thermal lag effects (see above) allowed us to ensure that the dependence of corrected melting temperature on heating rate (for  $q \sim 10$  K/min) was negligible.<sup>4</sup>

Melting temperatures reported here correspond to peak temperatures of endothermic transitions. Heats of fusion of isothermally crystallized samples were estimated through the following subtraction method. After appropriate thermal treatment to erase previous thermal history, a given sample was crystallized at a temperature  $T_x$  for a period of time,  $t_x$  and heated from  $T_x$  to a temperature ca. 20 K above the final observed melting temperature. The experiment was repeated with the same sample for different times,  $t_x$  at the same crystallization temperature. From each heating trace, we subtracted the thermogram obtained after a residence time at  $T_x$ , which was sufficiently short that it showed no evidence of melting. This baseline subtraction approach is equivalent to approximating the specific heat capacity of the semicrystalline material by that of the supercooled melt in the melting region. This approach, when applied to a sample exhibiting a degree of crystallinity given by  $X_c$  and a melting range  $\Delta T$  wide yields an absolute error in crystallinity given by:

$$\Delta X_c \cong \frac{X_c (\bar{C}_p^L - \bar{C}_p^C) \Delta T}{2\Delta H_f^0} \quad (3.1)$$

In the above equation,  $\bar{C}_p^L$  and  $\bar{C}_p^C$  are the melt and crystal specific heat capacities at the crystallization temperature and  $\Delta H_f^0$  is the specific enthalpy of fusion of a perfect crystal. For a polyethylene sample with  $X_c = 50$  % and  $\Delta T = 30$  K, the error  $\Delta X_c$  is smaller than 1 %. To minimize  $\Delta T$ , recording of the melting trace was initiated at the crystallization temperature. The lower the degree of crystallinity, the smaller the expected systematic error in the estimated crystallinity.

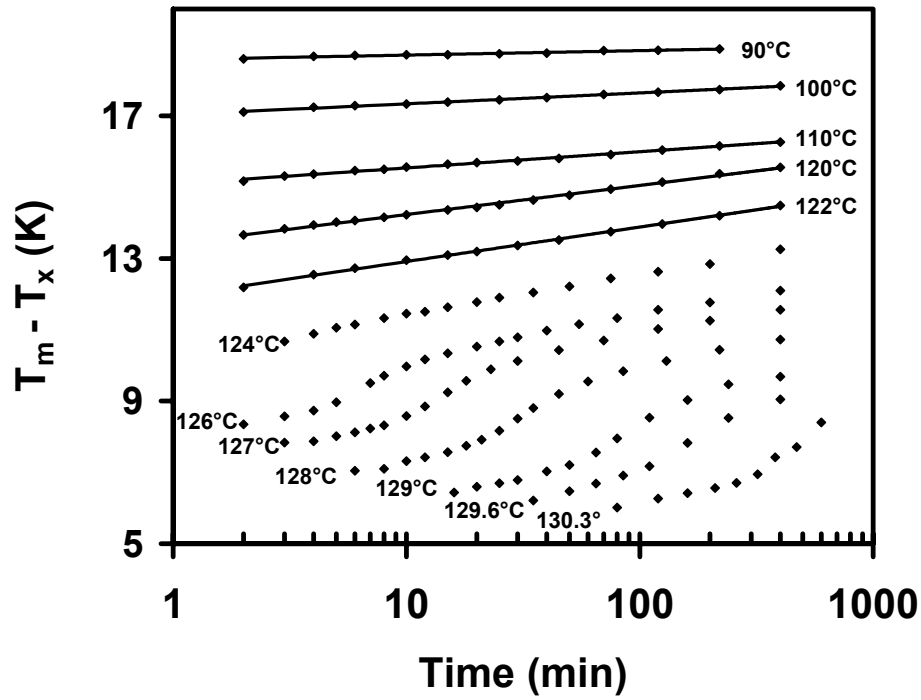
### 3.3 Results and Discussion

In the case of crystallization of PE-119K at high temperature, the melting point increases with time in sigmoidal fashion as shown in Figure 3.1(a). Similar observations were reported by Phillips et al. for poly( $\epsilon$ -caprolactone)<sup>3</sup> and Xu for polyoxyethylene,<sup>4</sup> two other linear flexible polymers. In the case of treatment at the lowest temperatures ( $T_x$ : 90–122 °C) the peak melting temperature increases linearly with the logarithm of residence time at these temperatures. In this latter case, the primary stage of crystallization is actually completed during cooling and evolution of the melting behavior with residence time at the indicated temperatures reflects the effect of secondary crystallization. Crystallization at intermediate temperatures (124–128 °C) leads to an intermediate behavior. The melting temperature increases initially in sigmoidal fashion and subsequently linearly with the logarithm of time.

We note that the evolution of the degree of crystallinity with time at these high crystallization temperatures also exhibits a sigmoidal shape, as shown in Figure 3.1(b). This observation leads us to speculate that the evolutions of the melting temperature and degree of crystallinity during isothermal crystallization are correlated. We now propose a simple model that is able to quantitatively describe the sigmoidal shape of the melting temperature evolution. At the core of this model is the assumption that the apparent DSC melting temperature can be approximated by the weight-average melting temperature of crystals formed at different times and thickened to different degrees. The shift of the apparent melting temperature with time is determined by the intrinsic rates of nucleation and growth (i.e., the rate of primary crystallization) and lamellar thickening.

We assume that we can describe the crystallization process as a sequence of three stages. In the first stage, primary crystallization takes place from the free melt, leading to the formation of new lamellar crystals. Spherulitic impingement marks the onset of the second stage. At this point, the significant reduction in the volume fraction of free melt leads to a marked decrease in the rate at which new lamellae are formed. During this intermediate stage, an increasing contribution to the change in the degree of crystallinity arises from the lamellar thickening process. This stage can be viewed as a mixed primary/secondary crystallization stage. Finally, the third stage is reached when the rate of primary crystallization becomes negligible compared to the rate at which crystallinity

(a)



(b)

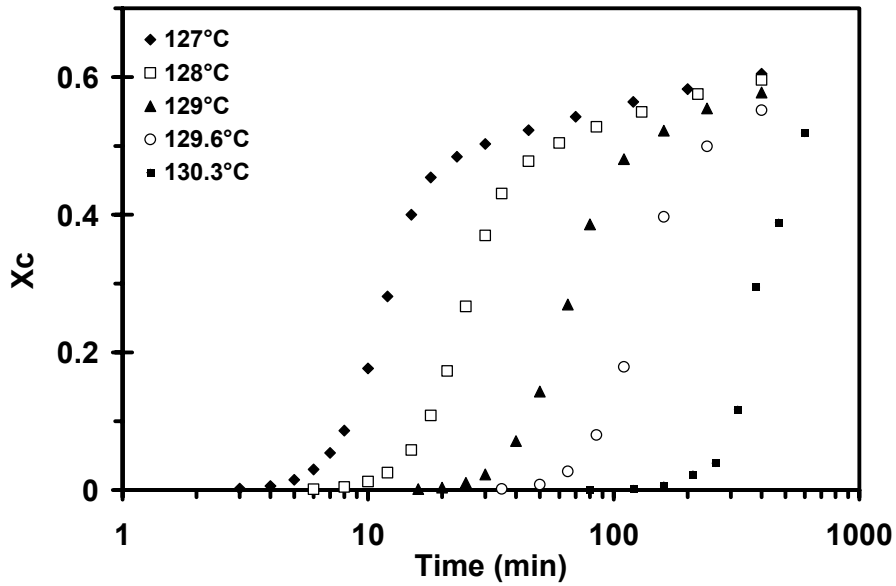


**Figure 3.1** Evolution of the difference between melting and crystallization temperatures (a) and evolution of the degree of crystallinity (b) as a function of residence time at the indicated temperatures. Data in (a) were arbitrarily shifted along the temperature axis for the sake of clarity.

increases through the lamellar thickening process. This third stage is a pure secondary crystallization stage.

To understand the role of lamellar thickening in the evolution of crystallinity during isothermal crystallization, we need to deconvolute the secondary crystallization from the primary process.

Primary crystallization of flexible polymers is well described by a two-step mechanism involving the nucleation of a crystalline phase from the undercooled melt and the subsequent linear growth of lamellar crystals from the initial crystalline seed.<sup>5,6</sup> These lamellae often twist, splay, and undergo noncrystallographic branching, resulting in the formation of a three-dimensional semicrystalline superstructure. If lamellar growth is allowed to proceed unhindered for a sufficient length of time, the resulting superstructure can develop the spherical symmetry characteristic of spherulites.

We consider a sample of mass,  $m^*$  cooled to a temperature  $T_x$  below the equilibrium melting temperature,  $T_m$ . As crystallization proceeds, the degree of primary crystallinity at time  $t$ , is given by  $X_c^p(t) = m_c^p(t) / m^*$ , where  $m_c^p(t)$  is the total mass of crystalline lamellae present at that time.

Under conditions where their thickening can be minimized (early stage of crystallization, crystallization at low temperature or from a good solvent), chain folded lamellar crystals are experimentally found to exhibit a narrow distribution of thicknesses. We will therefore assume that the initial distribution of lamellar thicknesses is monodisperse and that the material is well described during secondary crystallization by the evolution of the average initial thickness,  $l_c^0$ .<sup>7</sup> The degree of primary crystallinity can thus be written as

$$X_c^p(t) = \rho_c n_c(t) l_c^0 A_c / m^* \quad (3.2)$$

where  $\rho_c$ ,  $n_c(t)$ , and  $A_c$  are the crystal density, the total number of crystalline stems in the sample, and the chain cross-sectional area in the crystal phase, respectively. Isothermal primary crystallization can thus be simply described as a process leading to an increase in the number of crystalline stems of constant thickness,  $l_c^0$ . This process eventually slows down and ceases as lamellae from one spherulite impinge on lamellae from another spherulite. To model the increase in the number of crystalline stems or degree of

crystallinity with time, as simply as possible during primary crystallization, we will later on in this paper use the Avrami equation:<sup>8</sup>

$$X_c^P(t) = X_c^P(\infty) [1 - \exp(-kt^n)] \quad (3.3)$$

where  $X_c^P(\infty)$  is the limiting crystallinity associated with primary crystallization.

Polymers, unlike small molecules, never crystallize fully ( $X_c^P(\infty) < 1$ ). The liquid to crystal transformation can only take place at a measurable rate under conditions far removed from equilibrium. Under these conditions, crystallization occurs by a chain-folding process, and sections of polymer chains often end up trapped between neighboring lamellae as tie-chains (interlamellar bridges), cilia (dangling chain ends), or loops (loose or sharp folds) on the surface of a lamella. Tie chains, cilia and loops account for the existence of interlamellar amorphous regions. Polymers are therefore semicrystalline below their equilibrium melting temperature, in obvious violation of the Gibbs' phase rule. In an attempt to reach thermodynamic equilibrium, polymers continue to crystallize beyond the primary crystallization stage. This further increase in crystallinity is assumed here to take place solely by a mechanism of lamellar thickening (lamellar thickness increases above  $l_c^0$  in eq 3.2). For a description of other secondary crystallization processes (such as secondary crystal formation, lamellar insertion, etc.), the reader is referred to the relevant literature.<sup>9-12</sup>

Evidence for the isothermal thickening of lamellar crystals in polyethylene has been obtained indirectly by differential scanning calorimetry and small-angle X-ray scattering but was more convincingly demonstrated through Raman LAM measurements.<sup>13,14</sup> We assume that lamellae start to thicken as soon as they form and that the time dependence of their thickening can be described by the classical logarithmic law (eq 3.4):<sup>15-18</sup>

$$l_c(t', t) = l_c^0 \{1 + C \log(1 + [t - t']/\tau)\} \quad (3.4)$$

In the above equation,  $l_c(t', t)$  is the thickness at time  $t$  of a lamella formed at time  $t'$ ,  $C$  is a measure of the rate of thickening and  $\tau$  is a time constant.

We further assume that the total number of crystalline stems,  $n_c$ , is not affected by the secondary crystallization process, an approximation which should hold during bulk crystallization if the thickening is not too extensive. In support of this approximation, we recall that the small-angle X-ray long spacing recorded in situ during the isothermal

crystallization of polyethylene,<sup>19, 20</sup> polyoxyethylene,<sup>21</sup> and polyoxymethylene<sup>22</sup> is independent of crystallization time after primary crystallization. With these facts in mind, we make the simplifying assumption that the increase in crystal thickness occurs at the expense of the amorphous regions (by reeling in amorphous segments from loops, cilia and loose sections of tie chains).

Under these conditions, the rise in crystallinity associated with secondary crystallization simply originates from the increase in the lamellar thickness.  $dX_c^S(t', t)$ , the increment in crystallinity at time  $t$  during time  $dt$ , arising from the thickening of crystals formed at an earlier time  $t'$ , can be written as:

$$dX_c^S(t', t) = dX_c^P(t') C \log(1 + [t - t']/\tau) \quad (3.5)$$

Note that the term  $dX_c^P(t')$  in eq 3.5 describes the increment in primary crystallinity associated with the increase in number in crystalline stems,  $n_c(t')$ , at time  $t'$ . This amount of crystallinity increases by a factor  $C \log(1 + [t - t']/\tau)$  between time  $t'$  and  $t$  due to the corresponding increase in lamellar thickness (eq 3.4). The quantity  $dX_c^S(t', t)$  is therefore proportional to both the amount of crystal formed at time  $t'$  during time  $dt'$  and  $l_c(t', t) / l_c^0$ , the relative increment in lamellar thickness between  $t'$  and  $t$ .

Integration by parts of eq 3.5 leads to

$$X_c^S(t) = -C \int_0^t X_c^P(t') \left( \frac{d \log \left[ 1 + \frac{t - t'}{\tau} \right]}{dt'} \right) dt' \quad (3.6)$$

When the time,  $t$ , is much longer than the times over which changes in primary crystallinity can be observed,  $X_c^S(t)$ , the secondary crystallinity at time,  $t$ , is approximated by

$$X_c^S(t) \cong X_c^P(\infty) C \log(t/\tau) \quad (3.7)$$

The overall degree of crystallinity,  $X_c^T(t)$ , is equal to the sum of primary and secondary crystallinities at time  $t$ . Since the degree of primary crystallinity at long time is well approximated by its asymptotic value, we can express the overall degree of crystallinity in the long time limit as

$$X_c^T(t) = X_c^P(t) + X_c^S(t) \cong X_c^P(\infty) + X_c^P(\infty) C \log(t/\tau) \quad (3.8)$$

While use of the above equation could allow us to determine the constant  $C$  from a plot of  $X_c^T(t)$  vs.  $\log(t)$  at long times, this approach is only accurate if experimental data are available much beyond the primary crystallization stage. A more accurate approach for the determination of  $C$  will be presented later and relies on the deconvolution of primary and secondary crystallization contributions.

We will now show for the simple lamellar thickening model described here, that the same constant  $C$  accounts for the evolution of the melting temperature with crystallization time.

The melting temperature at time  $t$  of a lamellar crystal of thickness,  $l_c(t', t)$  formed at time  $t'$  is obtained through the Gibbs-Thomson equation:

$$T_m(t', t) = T_m \left( 1 - \frac{2\sigma_e}{\Delta H_f^0 l_c(t', t)} \right) \quad (3.9)$$

where  $T_m$  is the equilibrium melting temperature,  $\sigma_e$  is the fold surface free energy and  $\Delta H_f^0$  is the thermodynamic heat of fusion for the perfect bulk crystal (values given in Table 3.1). At time  $t$ , the sample contains lamellar crystals of different thicknesses. The melting curve for the sample of interest will consist in the superposition of the melting endotherms associated with crystal populations of different thicknesses. Since a given crystal population contributes to the melting process in proportion to its weight fraction, we assume that the apparent observed melting temperature is approximately given by the weight-average melting temperature. The weight fraction at time  $t$  of lamellae formed between times  $t'$  and  $t' + dt'$  is given by  $dP(t', t)$ :

$$dP(t', t) = \frac{dX_c^T(t', t)}{X_c^T(t)} \quad (3.10)$$

Thus, the weight-average lamellar thickness at time  $t$  is given by

$$\bar{l}_c(t) = \int_0^t dP(t', t) l_c(t', t) = \frac{1}{X_c^T(t)} \int_0^t l_c(t', t) dX_c^T(t', t) \quad (3.11)$$

and the “weight-average” melting temperature at time  $t$  is given by

$$\bar{T}_m(t) = \int_0^t dP(t', t) T_m(t', t) = \int_0^t \frac{dX_c^T(t', t)}{X_c^T(t)} T_m(t', t) \quad (3.12)$$

which, using  $dX_c^T(t', t) = dX_c^S(t', t) + dX_c^P(t')$  in combination with eq 3.5 leads to:

$$\bar{T}_m(t) = \frac{I}{X_c^T(t)} \int_0^t \left( \frac{dX_c^P(t')}{dt'} \right) T_m(t', t) \left[ I + C \log \left( I + \frac{t-t'}{\tau} \right) \right] dt' \quad (3.13)$$

According to eq 3.13, the average melting temperature can be obtained from experimental data of  $X_c^T(t)$  and from the evolution of  $X_c^P(t)$ .

Let us show now that the degree of primary crystallinity,  $X_c^P(t)$ , can be obtained numerically from the overall degree of crystallinity,  $X_c^T(t)$ . Using eq 3.5, the overall crystallinity,  $X_c^T(t)$  at  $t$  is written as

$$X_c^T(t) = \int_0^t \frac{dX_c^P(t')}{dt'} \left( I + C \log \left( I + \frac{t-t'}{\tau} \right) \right) dt' \quad (3.14)$$

Eq 3.14 is a Volterra equation of the first kind, which has as its analogue a matrix equation of the form:

$$XT_K = \sum_{J=1}^K dXP_J C_{KJ} \quad (3.15)$$

where  $XT_K$  is the vector with coordinates equal to the total crystallinity at different times up to  $t_K$ ,  $dXP_J$  is the vector with coordinates equal to the time derivative of the primary crystallinity at times  $t_J < t_K$  and  $C_{KJ}$  are matrix components of value:

$$C_{KJ} = I + C \log \left( I + \frac{t_K - t_J}{\tau} \right) \quad \text{for } t_K \geq t_J \quad (3.16)$$

$$C_{KJ} = 0 \quad \text{for } t_K < t_J$$

The time derivative of the primary crystallinity  $dX_c^P(t')/dt'$  (vector of components  $dXP_J$ ) is thus easily obtained from the overall crystallinity,  $X_c^T(t)$ , by solving the above matrix equation (eq 3.15) by forward substitution, since  $XT$  is a triangular matrix. The degree of primary crystallinity is then calculated by numerical integration of  $dX_c^P(t')/dt'$ .

$C$  is obtained by examination of the time dependence of the calculated  $X_c^P(t)$ . As shown below, if the value chosen for  $C$  is too low (or too high), a monotonically increasing (or decreasing) function  $X_c^P(t)$  is obtained at long times. To illustrate this method, we have generated some artificial evolution of the total crystallinity,  $X_c^T(t)$ , assuming an Avrami form for primary crystallization and a logarithmic law for the lamellar thickening process. The parameters chosen are given in Table 3.1.  $X_c^P(t)$  and  $X_c^S(t)$  are calculated using eqs 3.3 and 3.6, respectively.  $X_c^T(t)$  is obtained by direct summation of  $X_c^P(t)$  and  $X_c^S(t)$ . The evolution of these quantities is shown in Figure 3.2

along with their asymptotic behavior at long times (given by eqs 3.7 and 3.8 for  $X_c^S(t)$  and  $X_c^T(t)$ ). Note that the slopes of the straight lines representing eqs 3.7 and 3.8 are equal to each other and to  $C X_c^P(\infty)$ .

**Table 3.1** Inputted parameters for calculation

quantity	magnitude
$K$	$6.0 \times 10^{-6} \text{ min}^{-4}$
$N$	4
$X_c^P(\infty)$	0.4
$C$	0.3
$\tau$	1 min
$\sigma_e$	$90 \text{ mJ/m}^2$
$\Delta H_f^\circ$	$290 \text{ J/cm}^3$
$T_m$	$145 \text{ }^\circ\text{C}$

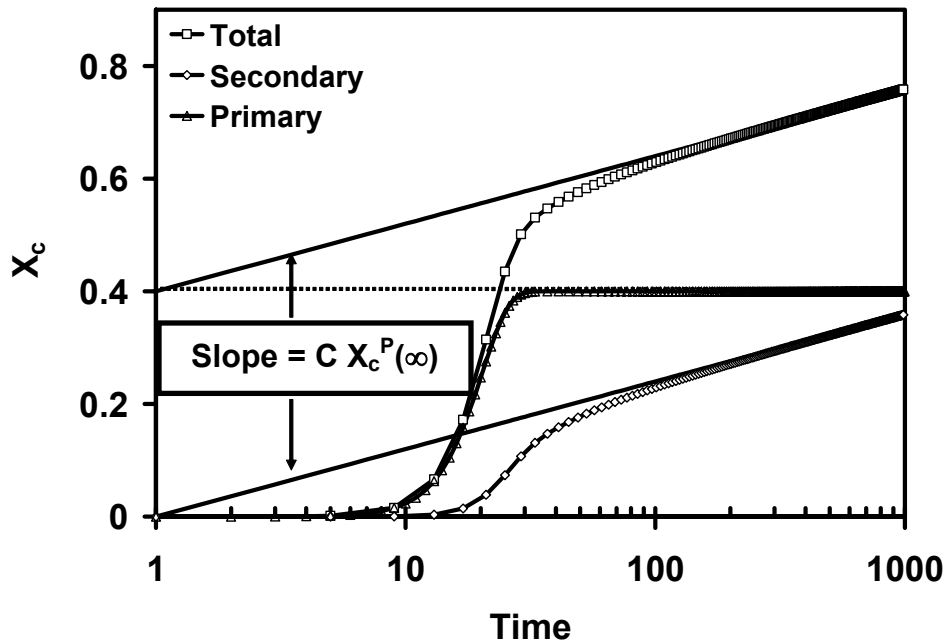


**Figure 3.2** Simulated primary ( $\Delta$ ), secondary ( $\diamond$ ), and total ( $\square$ ) crystallinity as a function of time. See text for details regarding their estimation.

As indicated earlier,  $X_c^P(t)$  is then calculated from the simulated  $X_c^T(t)$  by inversion of eq 3.15 and numerical integration. In Figure 3.3, we show the calculated  $X_c^P(t)$  for different choices of the quantity,  $C$ . The correct value of  $C$  is obtained (see inset on Figure 3.3) when the slope of  $X_c^P(t)$  at long times is equal to 0. From Figure 3.3, we conclude that the correct value of  $C$ , as expected from Table 3.1, must be equal to 0.3. Higher or lower  $C$  values do not produce a  $X_c^P(t)$  function which is constant at long times.

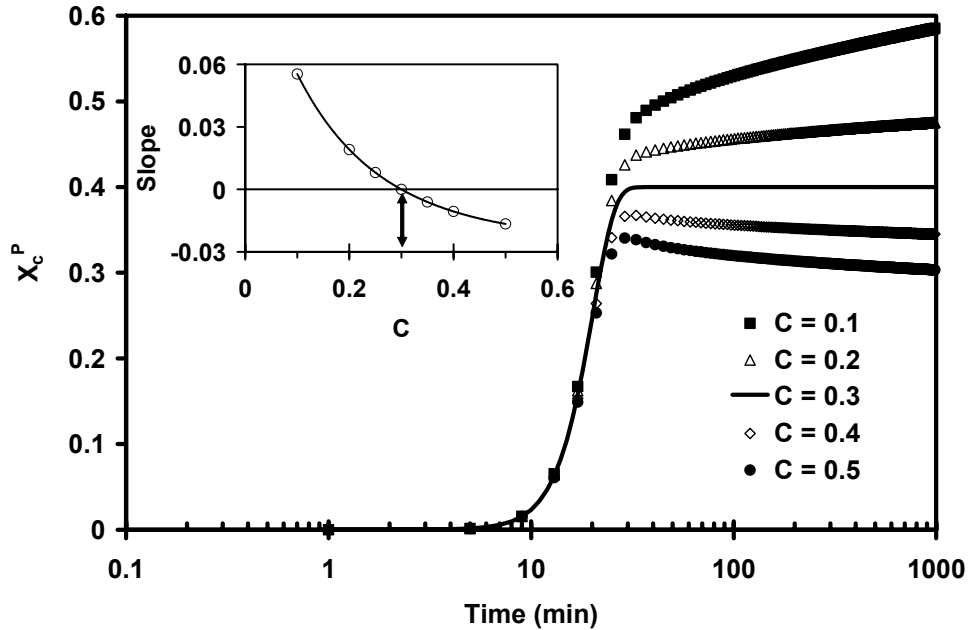
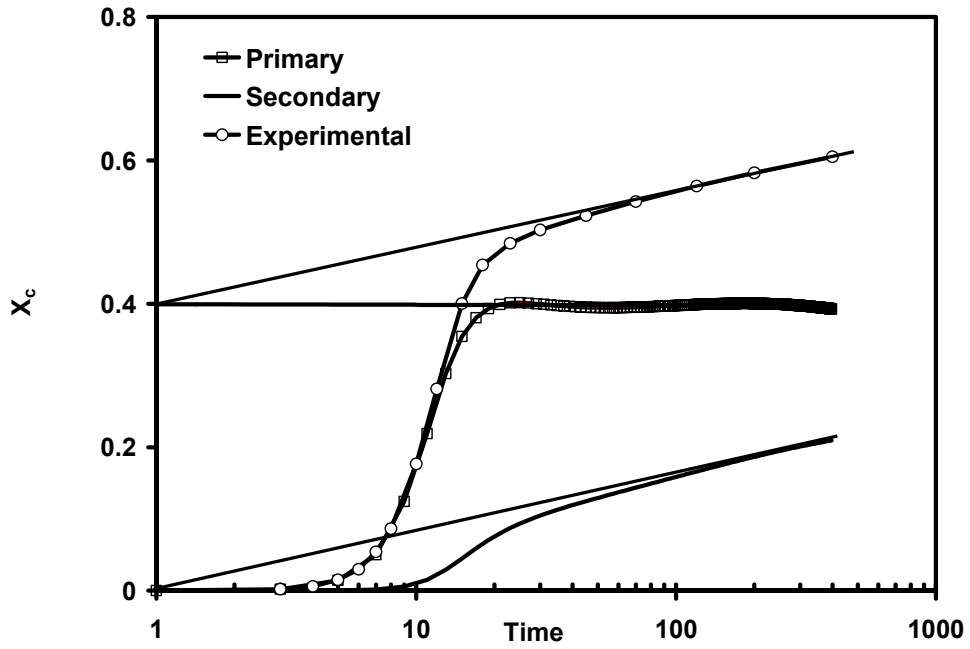


**Figure 3.3** Primary crystallinity calculated by solving eq 3.15 and subsequent numerical integration of  $dX_c^P(t)/dt$  for different choices of the parameter  $C$ . The insert shows the evolution of the slope,  $dX_c^P(t)/d\log t$  as a function of  $C$ . The slope was calculated for times  $t > 30$  min.

We now apply the above method (discussed in the context of Figure 3.3) to estimate the magnitude of  $C$  for isothermal crystallization at  $T_x = 127$  °C and  $T_x = 128$  °C. The evolutions of  $X_c^T(t)$ ,  $X_c^S(t)$  and  $X_c^P(t)$  are shown in parts a and b of Figures 3.4 for temperatures  $T_x = 127$  °C and  $T_x = 128$  °C where the values of  $C$  are found to be 0.203 and 0.237, respectively. We note, as expected, that the crystallinity at the early stage is

a



b

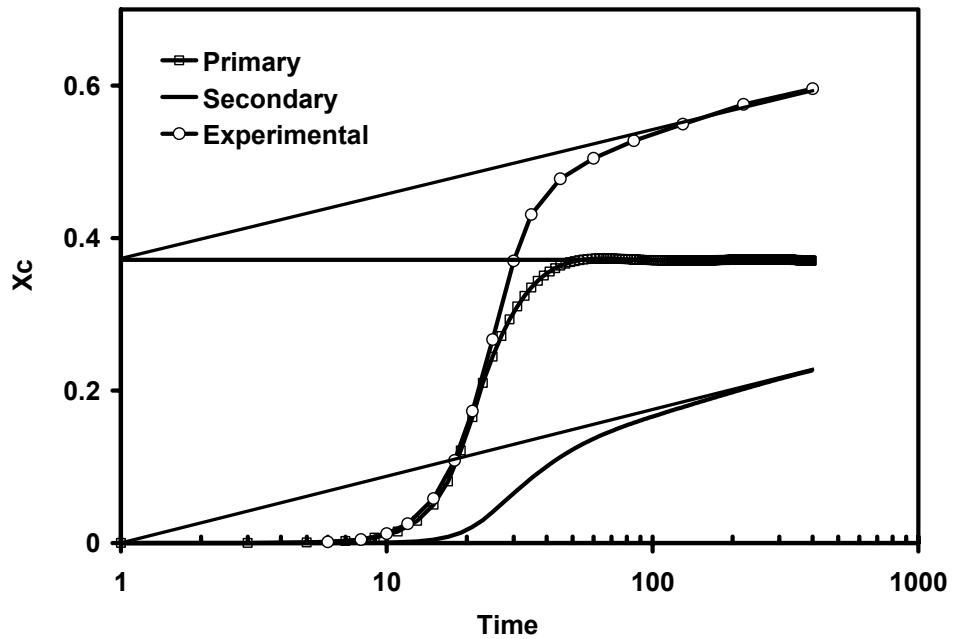
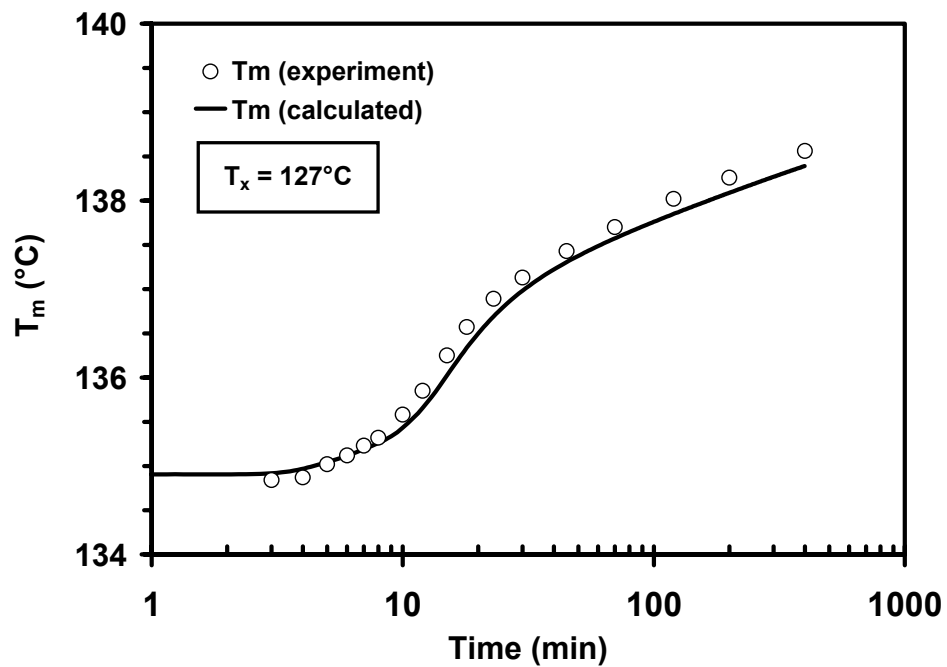


**Figure 3.4** Evolution of the fitted experimental crystallinity (o), calculated primary crystallinity ( $\square$ ), and calculated secondary crystallinity (full curve) with residence time at temperatures of 127 °C (a) and 128 °C (b).

mostly contributed by the primary crystallization and that primary crystallization is completed at these temperatures for  $t > \text{ca. } 50 \text{ min}$ . In this figure,  $X_c^P(t)$  was calculated using eqs 3.15 and 3.16, and  $X_c^S(t)$  was derived from  $X_c^S(t) = X_c^T(t) - X_c^P(t)$ . Note that eqs 3.6 and 3.8 fit the expected behavior of  $X_c^S(t)$  and  $X_c^T(t)$  at long times very well and that  $X_c^P(t)$  becomes constant after approximately 20 and 50 min at 127 and 128 °C, respectively.

$T_m(t',t)$  is calculated from the Gibbs-Thomson equation (eq 3.9), where the lamellar thickness,  $l_c(t',t)$  is estimated using eq 3.4. The only fitting parameter in this treatment is therefore  $l_c^0$ . parts a and b of Figures 3.5 show the comparison of simulated average melting temperatures (eq 3.13) with experimental melting temperatures for crystallization at  $T_x = 127 \text{ °C}$  and  $T_x = 128 \text{ °C}$ , respectively. As expected from the model, the experimental melting temperature in the early stage of primary crystallization is mostly controlled by the initial lamellar thickness ( $l_c^0 = 25.7 \text{ nm}$  at 127 °C and 25.5 nm at 128 °C). We find that for the above values of  $C$ , calculated melting temperatures fit the experimental melting temperature very well. This analysis suggests that the *same* logarithmic law can account for both the evolution of the secondary crystallinity and the evolution of the melting temperature with time. It also suggests that the empirical kinetic law used to describe the thickening process (eq 3.5) needs not consider two time regimes with different rates of thickening to account of the observed sigmoidal behavior, as was speculated by other researchers.<sup>17</sup> We note that while the initial lamellar thicknesses extracted by this analysis do not show the expected increase with decreasing undercooling, the rate of lamellar thickening (magnitude of  $C$ ) does increase with increasing temperature as expected for a process controlled by segmental mobility. In view of the rather narrow range of temperatures where crystallinity data can be analyzed, one should not be surprised by the lack of sensitivity of  $l_c^0$  to temperature. One should also note that the lamellar thicknesses derived from the above analysis are only slightly larger than those (20 - 22 nm) measured by Akpalu et al.<sup>23</sup> for a lower molar mass fraction polyethylene.

a



b

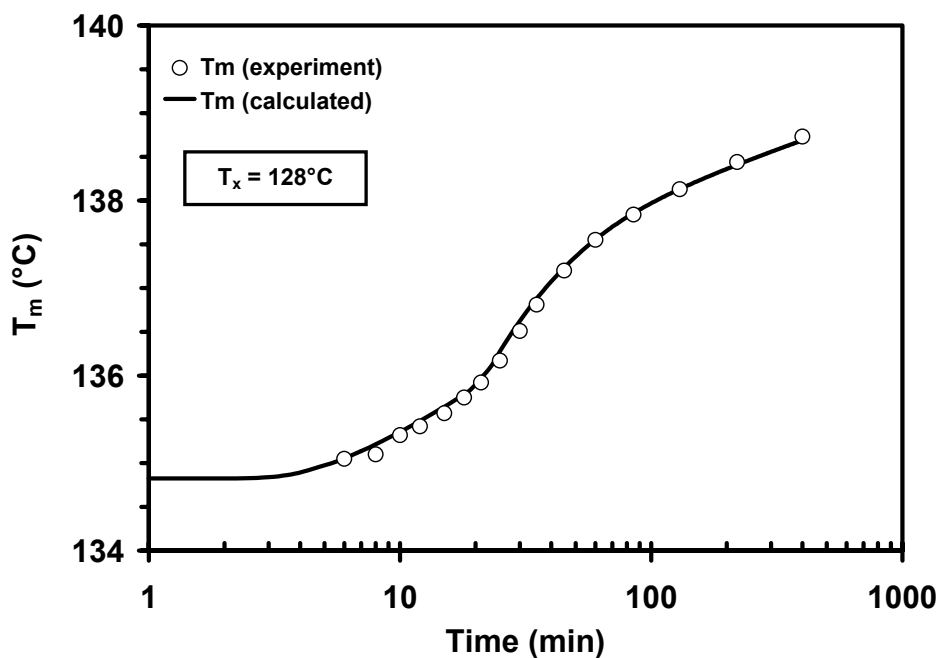


**Figure 3.5** Evolution of the experimental (o) and calculated (full curve) melting temperatures with residence time at temperatures of 127 °C (a) and 128 °C (b).

One of the possible shortcomings of this simplified model lies in the prediction that the melting range should become narrower at long time (see Figure 3.6). This prediction is not consistent with our experiments, which indicate that the width of the melting endotherm increases very slightly with crystallization time (see Figure 3.7). While this simplified analysis appears to successfully account for the sigmoidal evolution of the degree of crystallinity and average melting temperature with time, it certainly ignores the possibility that other mechanisms may be simultaneously at play. For instance, Phillips and Rensch<sup>3</sup> speculated that lamellar thickening might be a nucleated process, which would also lead to sigmoidal behavior. Other proposed mechanisms such as lamellar doubling,<sup>24-26</sup> which involve the overcoming of certain activation energy in the process of increasing lamellar thickness, may also obey some logarithmic law (eq 3.5), thus fulfilling the same empirical requirement in the model.

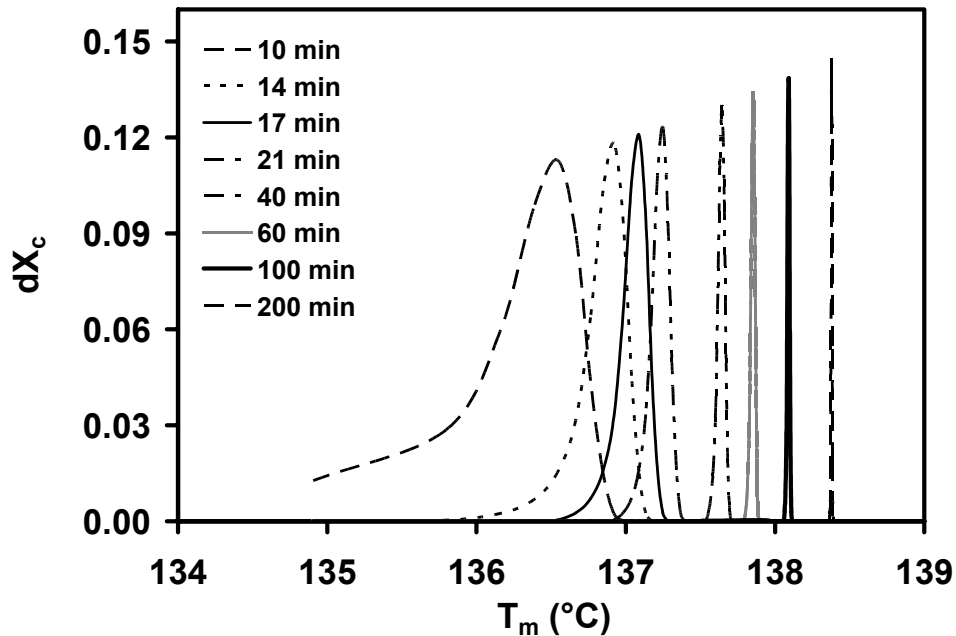


**Figure 3.6** Evolution of the calculated melting trace with crystallization time at 127 °C (crystallization times as indicated).  $dX_c$  is the fraction of crystallinity which melts at temperature  $T_m$ . Crystallinity increments and melting temperatures were calculated for time steps,  $dt' = 2$  min.

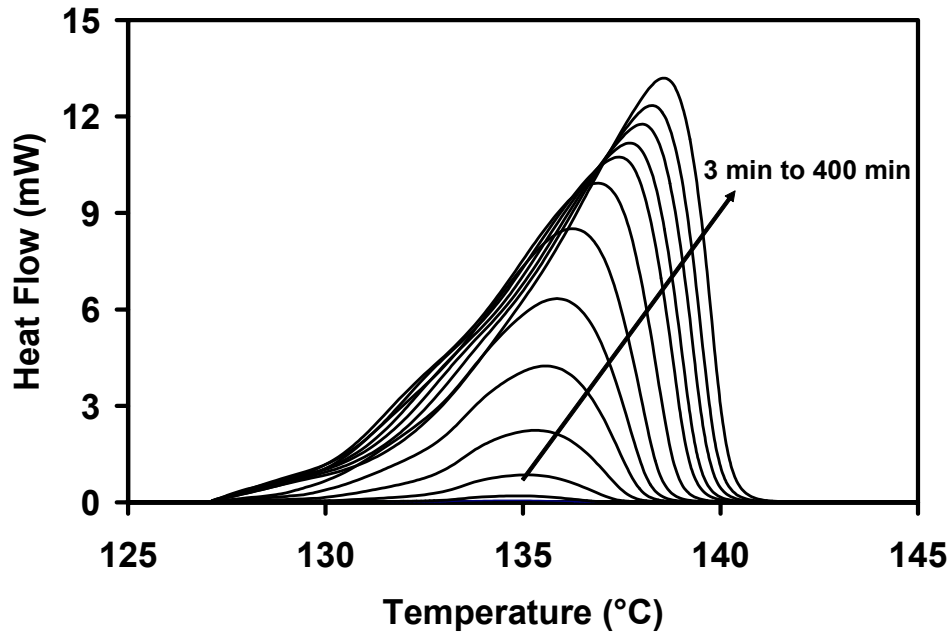


**Figure 3.7** Evolution of the experimental melting trace with crystallization time at 127 °C (crystallization times as indicated).

In this simple-minded model, we have assumed that the same rate law for thickening applies during the whole process of isothermal crystallization. While this logarithmic law is consistent with secondary crystallization data presented in Figures 3.1a for temperatures ranging from 90 to 120 °C, and with LAM data from Stack et al.,<sup>14</sup> theoretical studies by Sanchez et al.<sup>27, 28</sup> suggested that one should not expect it to be strictly valid at all crystallization times and temperatures. One can certainly envision that as thickening proceeds, tie chains in the interlamellar regions become more frustrated as they attempt to respond to the pull from neighboring lamellae. Along similar lines, one may envision that the disentanglement process required for the attainment of perfect crystalline order becomes more and more difficult, as constraints increase in the interlamellar amorphous regions. One should therefore expect that the kinetic parameters describing the thickening law differ from lamella to lamella and possibly for different parts of a single lamella. Whether such phenomena are actually at the origin of the empirical logarithmic law or require a different kinetic description of thickening at very long crystallization times cannot be answered by this study.

It is noted that Sanchez et al.<sup>27,28</sup> initially proposed a lamellar thickening model to explain the sigmoidal shape of the lamellar thickness evolution. The sigmoidal behavior originates in their model from the assumption that, at a given temperature, the lamellar thickness displays both lower and upper bounds. The upper bound is associated with the equilibrium value obtained by minimizing the overall (bulk + surface) free energy. The sigmoidal behavior assumed by the Sanchez theory is therefore intrinsically associated with the secondary crystallization process. This is in stark contrast with the claim, supported by the present analysis that the sigmoidal shape observed in the evolution of the lamellar thickness and the melting temperature with crystallization time is associated with the primary crystallization process.

### **3.4 Conclusions**

We have shown in the case of linear polyethylene that the increase in melting temperature with time during crystallization at high temperature can be quantitatively accounted for by a simple model that considers the kinetics of primary crystallization and assumes that lamellar thickening is well described by the classical semiempirical logarithmic law.

This model also specifically explains the similar sigmoidal shapes observed in the evolution of both the degree of crystallinity and the melting point at short times and at high crystallization temperatures. Support for this model is suggested by the observation that the same kinetic parameters can quantitatively describe the linear increase in both the melting temperature and the secondary crystallinity with the logarithm of time. Finally, we proposed a method enabling the deconvolution of primary and secondary crystallinity contributions to the overall degree of crystallinity.

### 3.5 Reference

---

- (1) Boyd, R. H. *Polymer* **1985**, *26*, 1123.
- (2) Hu, W. -G.; Boeffel, C.; Schmidt-Rohr, K. *Macromolecules* **1999**, *32*, 1611.
- (3) Phillips, P. J.; Rensch, G. J. *J. Polym. Sci., Part B: Polym. Phys.* **1989**, *27*, 155.
- (4) Xu, J. N. Ph.D. Thesis, Virginia Polytechnic Institute and State University, **1999**.
- (5) Khoury, F.; Passaglia, E. In *Treatise on Solid State Chemistry*; Hannay, N. B., Ed.; Plenum, New York, 1976; Vol. 3, Chapter. 6.
- (6) Bassett, D. C. *Principles of Polymer Morphology*; Cambridge University Press: Cambridge, 1981.
- (7) Hoffman, J. D.; Davis, G. T.; Lauritzen, J. I. Jr., In *Treatise on Solid State Chemistry*; Hannay, N. B., Ed.; Plenum, New York, 1976; Vol. 3, Chapter. 7.
- (8) Avrami, M. *J. Chem. Phys.* **1939**, *7*, 1103.
- (9) Alizadeh, A.; Richardson, L.; Xu, J.; McCartney, S.; Marand, H.; Cheung, Y. W.; Chum, S. *Macromolecules* **1999**, *32*, 6221.
- (10) Marand, H.; Alizadeh, A.; Farmer, R.; Desai, R.; Velikov, V. *Macromolecules* **2000**, *33*, 3392.
- (11) Alizadeh, A.; Sohn, S.; Quinn, J.; Marand, H.; Shank, L. C.; Iler, H. D. *Macromolecules* **2001**, *34*, 4066.
- (12) Strobl, G. R.; Engleke, T.; Meier, H.; Urban, G. *Colloid Polym. Sci.* **1982**, *260*, 394.
- (13) Duglosz, J.; Fraser, G. V.; Grubb, D.; Keller, A.; Odell, J. A.; Goggin, P. L. *Polymer* **1976**, *17*, 479.
- (14) Stack, G. M.; Mandelkern, L.; Voigt-Martin, I. G. *Polym. Bull.* **1982**, *8*, 421.
- (15) Fischer, E. W.; Schmidt, G. F. *Angew. Chem. Internat. Ed.* **1962**, *1(9)*, 448.
- (16) Fischer, E. W. *Pure Appl. Chem.* **1972**, *31*, 113.
- (17) Weeks, J.J. *J. Res. Nat. Bur. Stds.* **1963**, *67A*, 441.
- (18) Hoffman, J. D. *Soc. Plast. Eng. Trans.* **1964**, *4*, 315.
- (19) Bark, M.; Zachmann, H. G.; Alamo, R.; Mandelkern, L. *Makromol. Chem.* **1992**, *193* 2363.
- (20) Akpalu, Y. A.; Amis, E. J. *J. Chem. Phys.* **2000**, *113*, 392.
- (21) Talibuddin, S.; Runt, J.; Liu, L. Z., Chu, B. *Macromolecules* **1998**, *31*, 1627.

- 
- (22) Yeh, F.; Hsiao, B.S.; Chu, B.; Sauer, B.B.; Flexman, E.A. *J. Polym. Sci. Polym. Phys. Ed.* **1999**, *37*, 3115.
- (23) Akpalu, Y. A.; Amis, E. J. *J. Chem. Phys.* **1999**, *111*, 8686.
- (24) Barham, P. J.; Keller, A. *J. Polym. Sci. Polym. Phys. Ed.* **1989**, *27*, 1029.
- (25) Loos, J.; Tian, M.; Rastogi, S.; Lemstra, P. J. *J. Mater. Sci.* **2000**, *35*, 5147.
- (26) Rastogi, S.; Spoelstra, A. B.; Goossens, J. G. P.; Lemstra, P. J. *Macromolecules* **1997**, *30*, 7880.
- (27) Sanchez, I. C.; Colson, J. P.; Eby, R. K. *J. Appl. Phys.* **1973**, *44*, 4332.
- (28) Sanchez, I. C.; Peterlin, A.; Eby, R. K.; McCrackin, F. L. *J. Appl. Phys.* **1974**, *45*, 4216.